Molecular Catalysis 501 (2021) 111376

Contents lists available at ScienceDirect

Molecular Catalysis

journal homepage: www.journals.elsevier.com/molecular-catalysis

Solvent-free elaboration of Ni-doped MnO_x catalysts with high performance for NH_3-SCR in low and medium temperature zones

Hui Kang [a], Jiajie Wang [a], Jian Zheng [a], Wei Chu [a,*], Changjin Tang [b], Ji Jiawei[b], Rui Ren [a], Mengxia Wu [a], Fangli Jing [a,*]

[a] School of Chemical Engineering, Sichuan University, Chengdu, 610065, PR China
[b] Key Laboratory of Mesoscopic Chemistry of MOE, School of Chemistry and Chemical Engineering, Nanjing University, Nanjing, 210093, PR China

ARTICLE INFO

Keywords:
NiO-MnOx catalyst
Solvent-free preparation
NH_3-SCR
NO removal
Heterogeneous catalysis

ABSTRACT

Cryptomelane-type Ni-doped MnOx catalysts (NMOs) prepared by solvent-free doping method showed very attractive performances in wide temperature zones and stability for selective catalytic reduction (SCR) at 100–300 ℃. The effect of Ni loading on NH_3-SCR activity at medium temperature (200–300 ℃) was investigated. The NMOs-4 catalyst not only maintained excellent low temperature (100–200 ℃) NH_3-SCR activity, the NO conversion was approached to 100 %, but also significantly improved the medium temperature activity while the NO conversion increased from 54.4% to 87.2% at 300 ℃ (T_{95} = 100–265 ℃) compared with undoped MOs catalyst (T_{95} = 100–225 ℃). Appropriate Ni loading could effectively tune the surface lattice oxygen activity and acidity of catalyst to ensure the NH_3 activation ability at low temperature and inhibit the occurrence of NH_3 direct oxidation at higher temperature. On other words, moderate NH_3 activation capacity was the key to achieve a wide temperature region of MnOx-based catalysts.

1. Introduction

Nitrogen oxides (NOx: including NO and NO_2) are emitted by chemical or combustion processes, which have great direct damaging effects on human health and the ecosystem [1]. Moreover, the interaction of NOx, volatile organic compounds (VOCs) and sunlight will also cause the surface ozone which is another toxic air pollutant [2]. It is necessary to control the NOx emissions. Selective catalytic reduction with NH_3 (NH_3-SCR) is the most promising technology by reducing the NOx to N_2 [3]. It mainly involves the following reactions (Eq. 1∼5) [4]. The V-based catalyst (V_2O_5-WO_3(MoO_3)/TiO_2) is commonly used in industry but its working temperature region (300–400 ℃) is too narrow to apply to low temperature (100–300 ℃) denitrification process [5]. Furthermore, the main active component of V-based catalyst is V_2O_5 which is easy to sublimate in the process of use, resulting in the secondary pollution and other problems. It becomes quite necessary to replace the industrial V-based NH_3-SCR catalysts with other transition metal oxide ones with excellent low temperature activity and wide active temperature region simultaneously.

$$4NH_3+4NO + O_2 \rightarrow 6H_2O+4N_2 \quad (1)$$

$$4NH_3+2NO_2+O_2 \rightarrow 6H_2O+3N_2 \quad (2)$$

$$4NH_3+2NO+2NO_2 \rightarrow 6H_2O+4N_2 \quad (3)$$

$$4NH_3+6NO \rightarrow 6H_2O+5N_2 \quad (4)$$

$$8NH_3+6NO_2 \rightarrow 12H_2O+7N_2 \quad (5)$$

$$NH_3+O_2 \rightarrow H_2O + NO_x \quad (6)$$

Active sites show their significant dependence on active temperature region. MnOx-based [6] or CuOx-based [7] catalysts are usually used in low temperature (<200 ℃) NH_3-SCR process. Whereas the CeOx-based [8], FeOx-based [9,10] and VOx-based [11] are mainly used in medium and high temperature (>200 ℃) processes. The MnOx-based catalysts have recognized excellent NH_3-SCR activity at low temperature [12–17], high NO removal efficiency can be achieved even below 150 ℃ [18,19]. However, MnOx-based catalysts have a narrow active temperature region and the NO conversion decreases obviously when the reaction temperature increases to 200–300 ℃ [6,15,18]. This is not conducive to the application of MnOx-based catalysts in flue gas purification with large temperature fluctuations, and it's significant to

* Corresponding authors.
E-mail addresses: chuwei1965@scu.edu.cn (W. Chu), fangli.jing@scu.edu.cn (F. Jing).

https://doi.org/10.1016/j.mcat.2020.111376
Received 20 October 2020; Received in revised form 11 December 2020; Accepted 14 December 2020

broaden the active temperature region of MnOx-based catalysts.

The main reason for the decrease of NO conversion at medium and high temperature reported in the literature is the direct oxidation of NH_3 (Eq. 6) [6,9,20], which competes with the NH_3-SCR reactions (Eq. 1∼5) at higher temperature [9,21], resulting in the loss of reducing agent and the decrease of NO conversion. Inhibiting the direct oxidation of NH_3 at high temperature is helpful to broaden the active temperature region [22–25]. It has reported that the introduction of strong acid site is the key to improve the NH_3-SCR performance at medium and high temperature [23,25,26]. Shen et al. [23] regulated the number and strength of acidic site by introducing a variety of transition metals (Zr, Fe, Cu, Ni, Mn) into TiCeOx catalysts. The results showed that the strong acid site on the surface of catalyst was beneficial to the movement of active temperature region to the high temperature region. In addition, some researchers found that SO_2 treatment can effectively generate strong acid site on catalyst surface and significantly improve the denitrification activity at high temperature [25,26]. The introduction of strong acid site can enhance the adsorption strength of NH_3, thus reducing the activation and transformation of NH_3. However, from the characterization results of the above literatures, it was also found that the introduction of acid site weakens the redox ability of catalyst at the same time. Therefore, it is not clear which is the more important factor between acidity and redox ability to affect the medium and high temperature activity. Obviously, the bifunctional catalyst possessing simultaneously acidity and redox properties was necessary to catalyze NH_3-SCR reaction. The surface acidic site was helpful for the adsorption NH_3 molecules, and the redox property was in favor of the activation adsorbed NH_3 [27,28]. Thus, the coordination between the acidity and redox became very important to develop an efficient catalyst.

In this work, MnOx catalyst (MOs) with excellent low-temperature NH_3-SCR activity was synthesized by solvent-free method, while the NH_3-SCR activity decreased obviously when the reaction temperature was above 200 ℃. The medium temperature (200–300 ℃) NH_3-SCR activity of MnOx-based catalyst was effectively improved through the solvent-free Ni doping. And the balance between low temperature activity and medium-high temperature activity of the catalyst was achieved by tuning the Ni loading. The Ni doped MnOx-based catalyst with excellent NH_3-SCR activity at 100–300 ℃ was obtained. It was found that weakening the redox ability played a more important role than controlling the acidity for the improvement of medium temperature activity.

2. Experimental

2.1. Catalysts preparation

The MnOx-based catalysts were synthesized by a solvent-free method [29]. Solid phase $KMnO_4$ (99.5 %, AR) and $Mn(CH_3COO)_2{\cdot}4H_2O$ (99.0 %, AR) were mixed at a molar ratio of 2: 3. The mixture was ground in a mortar for 20 min, and then transferred to an 80 ℃ oven for 4 h. The resulting solid was washed with deionized water and filtered until the filtrate was colorless and transparent, and finally dried in an 80 ℃ oven overnight to obtain the catalyst labeled as MOs. The MOs calcined at different temperatures for 3 h was labeled MOs-T (T = 300, 350, 400 and 500 ℃). As a contrast, MnOx catalyst was synthesized by hydrothermal method, and labeled as MO-HT. The detailed process was described in the supporting information.

A series of Ni-doped MnOx catalysts was synthesized by solvent-free doping method. A certain proportion of $Ni(CH_3COO)_2$ (98.0 %, AR) was added in the solid phase mixing step in the process of MOs synthesis, and the other steps remained unchanged. Ni-doped MnOx catalysts were labeled as NMOs-1, NMOs-2, NMOs-3, NMOs-4, NMOs-5 and NMOs-6, where the Ni/Mn molar ratios were 0.06, 0.13, 0.29, 0.50, 0.78 and 1.75, respectively. And the more detail was shown in Table S1 in Supporting information.

2.2. Catalyst characterization

The X'Pert Pro MPD DY129 of Holland Panalytical Empyrean diff ; ractometer was used for X-ray diffraction (XRD) test (Cu Kα radiation, 40 kV, 35 mA). Fourier transform infrared (FT-IR) spectroscopy was used to confirm the crystal structure using Spectrum Two Li10014. The bulk atomic concentrations were measured by X-ray energy dispersive spectroscopy (EDS) linked with scanning electron microscopy (SEM). The BET specific surface area of catalyst was measured by nitrogen adsorption at 77 K using a NOVA 1000e of Quantachrome Company. The pore size distribution was obtained from the N_2 desorption isotherm using the BJH method. X-ray photoelectron spectroscopy (XPS) was performed on a XSAM 800 instrument accompanied by a Mg Kα radioactive source. H_2 temperature programmed reduction (H_2-TPR) experiments were conducted on TP-5080 Adsorption instrument using 50 mg of catalysts. The sample was pretreated at 300 ℃ for 1 h in N_2 flow. The test temperature region was 50–600 ℃ at a heating rate of 10 ℃ min^{-1} with 10 % H_2/Ar gases. NH_3 temperature programmed desorption (NH_3-TPD) experiments were carried out on Thermofisher IS10 FTIR spectrometer using 50 mg of catalysts which were pretreated at 300 ℃ with Ar for 30 min followed by NH_3 adsorption to saturation and Ar purge at 50 ℃. The desorption was performed in Ar from 50 to 600 ℃ at a heating rate of 10 ℃/min.

2.3. NH_3-SCR catalytic activity test

The NH_3-SCR activity of the catalysts was tested in a fixed bed reactor (quartz, inner diameter: 8 mm) at atmospheric pressure while the reaction temperature varied in the range of 100–350 ℃ with catalysts sieved to 40–60 mesh. The composition of simulated flue gas included 500 ppm NO, 500 ppm NH_3, 5 vol.% O_2, and Ar as balance. The total gas flow rate was 100 mL/min over 50−200 mg of catalysts. The concentration of NO was detected by FGA-4100. All data were collected after the NO concentration of the outlet of the reactor was stable. The NO conversion (X_{NO}) was calculated by Eq. (7):

$$X_{NO} = \frac{n_{NO,in} - n_{NO,out}}{n_{NO,in}} \times 100\% \quad (7)$$

Where $n_{NO,in}$ and $n_{NO,out}$ refer to the molar quantity of NO at inlet and outlet, respectively. The stability test of the catalyst was basically consistent with that of NH_3-SCR activity tests. The catalytic stability was performed at 200 ℃ with a weight hourly space velocity of 30,000 mL/g h

2.4. NH_3 oxidation reaction activity test

The direct oxidation ($NH_3 + O_2$) ability of catalysts was tested at 150 ℃. The feed gas consisted of 500 ppm NH_3 (5 vol.% O_2 in N_2) with a total flow rate of 100 mL/min over 100 mg of catalysts. The concentration of NH_3 was detected by Thermofisher IS10 FTIR spectrometer. Similarly, the oxidation conversion of NH_3 was obtained by calculating the concentration change of NH_3 at the inlet and outlet.

3. Results and discussion

3.1. Catalyst composition by XRD and FT-IR

X-ray diffraction (XRD) patterns of calcined catalyst MOs-350 and uncalcined catalysts MOs and NMOs with different Ni loading were obtained and shown in Fig. 1A. The obvious diffraction peaks at 28.7°, 37.5°, 42.0°, 49.9°, 60.2° for the sample MOs-350 were assigned to cryptomelane-type manganese oxides (KMn_8O_{16}, JCPDS: PDF#29−1020) involving a 2 × 2 pore structure [29,30]. The uncalcined catalysts showed poor crystallinity, only showing a broad diffraction at 37.5°. Comparing with the liquid phase synthesis, the solid

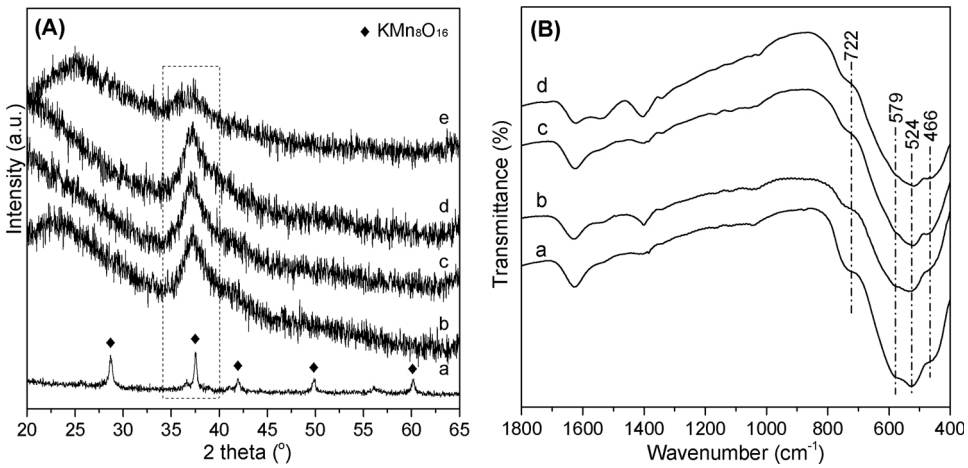

Fig. 1. (A) XRD patterns (a: MOs-350, b: MOs, c: NMOs-1, d: NMOs-4 and e: NMOs-6) and (B) FT-IR spectra for catalysts (a: MOs, b: NMOs-1, c: NMOs-4 and d: NMOs-6).

reaction tended to occur at the interface, the resulting nanoparticles were small and distributed narrowly [31]. Furthermore, these species were difficult to move and aggregate freely without thermal treatment [32,33], the corresponding diffraction should be weak. Therefore, It could be speculated that the broad diffractions at 37.5° for uncalcined samples originated from cryptomelane-type manganese oxides using sample MOs-350 as a reference.

In addition, it was also observed that the diffraction peak intensity at 37.5° for the Ni excessively doped NMOs-6 catalyst significantly reduced, which may be due to the decreasing of surface MnOx content or the catalyst particle size. On the other hand, no XRD diffraction peaks of Ni species were detected in all Ni-doped catalysts, indicating that Ni species might have a good dispersion or incorporate into the crystal lattice.

In order to further verify the crystal type of the catalysts, infrared spectroscopy was performed at room temperature. The four catalysts showed the infrared absorption bands at 772, 579, 524, and 466 cm^{-1} from Fig. 1B, which belonged to the Mn-O vibration of MnO_6 octahedral framework in cryptomelane-type manganese oxide [34]. This also confirmed that the MOs and NMOs catalysts synthesized by solvent-free method existed mainly in the form of cryptomelane-type manganese oxide.

3.2. Porosity by N_2 adsorption/desorption isotherms

Fig. 2 showed the N_2 adsorption/desorption isotherms and pore size distribution of the catalysts. All catalysts exhibited a typical type-IV isotherm according to the definition of IUPAC [35,36], which was one of the main characteristics of mesoporous materials. MOs catalyst had H3 type hysteresis loop and no obvious saturated adsorption platform, indicating that the pore structure was irregular sheet-like. While the H2 type hysteresis loop was found for Ni-doped catalysts, suggesting the transformation of pore structure through the introduction of Ni species. The evident difference could be also seen from the pore size distribution diagram, the MOs catalysts had a wide pore size distribution in the range of 3−80 nm. The addition of Ni species made the distribution become narrower, and it could be easily tuned by the changing the content of Ni species. As a result, NMOs-1, NMOs-4 and NMOs-6 exhibited the distribution of 2–6, 2–10 and 2−20 nm, respectively.

More specifically, the BET specific surface area (SSA), pore volume and pore diameter were reported in Table 1. Compared with

Table 1
BET specific surface area, pore characterization and T95 performance of the catalysts.

Catalysts	S_{BET}, (m^2/g)	Pore Volume, (cm^3/g)	Pore diameter, (nm)	T_{95} (℃)
MOs	131.2	0.33	10.0	100−225
NMOs-1	75.4	0.18	9.7	100−217
NMOs-4	105.2	0.18	6.8	100−265
NMOs-6	143.0	0.19	5.2	121−217

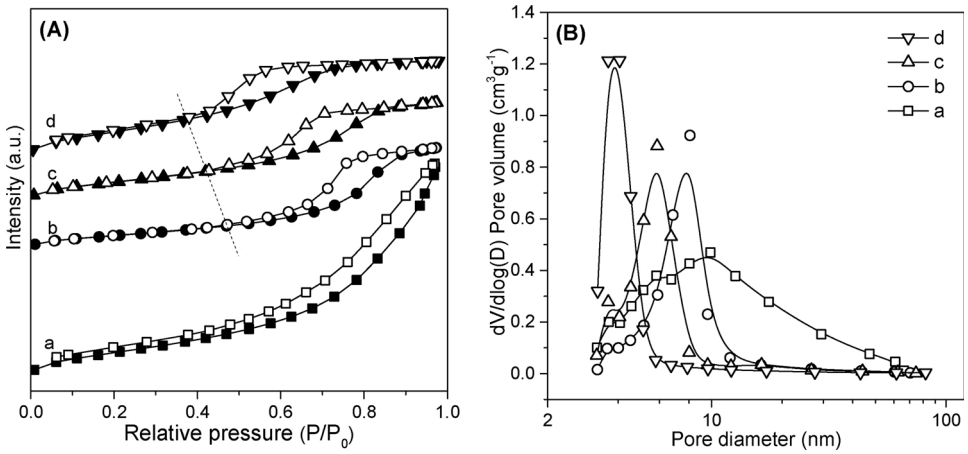

Fig. 2. N_2 physisorption isotherms (A) and pore size distribution (B) of different catalysts (a: MOs, b: NMOs-1, c: NMOs-4 and d: NMOs-6).

hydrothermal and reflux methods [30,37,38], the MOs synthesized by solvent-free method had a smaller particle size, so that the catalyst had a larger specific surface area of 131.2 m^2/g. For Ni doped catalysts, the Ni loading had a significant effect on SSA. The SSA of NMOs-1, NMOs-4, NMOs-6 catalysts were 75.4, 105.2 and 143.0 m^2/g, respectively. The pore volume of the catalysts dropped considerably due to the incorporation of Ni, but it (0.18−0.19 cm^3/g) did not change a lot as the varied Ni loading. In despite of that, the pore size decreased from 9.7 nm for NMOs-1 to 5.2 nm for NMOs-6 with the increase of the Ni loading, which could be inferred that Ni-containing species had formed new small pores in the pores of MnOx.

3.3. Bulk and surface composition of catalysts

Energy dispersive spectrometer (EDS) was used to test the bulk element composition of catalysts [30,39,40], the results were shown in Table 2. K and Mn were the metal elements in MOs catalyst where the K was partially substituted by Ni to give NMOs. It was interesting to note that the Mn content in NMOs-1 (32.6 %) catalyst with minimum loading of Ni did not change significantly comparing with that of MOs (30.7 %). With the further increase of Ni loading, it decreased to the comparable values of 26.4 % and 27.4 % for NMOs-4 and NMOs-6 catalysts, respectively.

X-ray photoelectron spectroscopy (XPS) was applied to measure the surface element composition, and the quantified data were listed in Table 2. The surface K content had the same changing trend as that of EDS analysis. Similarly, the surface Mn content was close to that of bulk Mn content when small quantity of Ni was added like in the sample NMOs-1, it decreased to 25.0 % for NMOs-4 and 17.4 % for NMOs-6 containing higher Ni content in catalysts. Obviously, the introduction of Ni made the surface element redistribute, the surface content of Ni increased with the increase of its loading, while surface K content correspondingly dropped down even became zero in NMOs-4 and NMOs-6. Such a change could be clearly observed from K2p and Ni2p XPS spectra (Fig. S1 in SI).

The Ni content whatever in bulk or on surface showed its dependence on its loading. It was worth noting that the designed Ni/Mn ratio was much larger than that in the final catalyst (Supporting information Table S1). Typically, the designed Ni/Mn ratio in NMOs-6 catalyst was 1.75, while it was actual only 0.24 based on the EDS result. In the ternary system of $KMnO_4$, $Mn(Ac)_2$ and $Ni(Ac)_2$, the redox reaction between $KMnO_4$ and $Mn(Ac)_2$ mainly occurred, $Ni(Ac)_2$ only participated in a quite limit extent, which could be concluded from XRD and FT-IR results as MnOx phase was mainly found. Ni partially replaced the K and Mn elements during the synthesis process, the pore structure transformed significantly from the sheet-like to ink bottle-like according to the isotherms, such a change ensured the Ni could be anchored in the pores cryptomelane-type manganese oxide species thanks to the oxygen-rich environment [19]. Furthermore, the external surface mainly exposed (111) crystal plane with an uneven semi-tunnel structure, which may also be the anchor sites of Ni species on the surface [15].

The O 1s spectra were fitted to investigate the different chemical environment of O species, the corresponding peak at *ca.* 529.5 eV were attributed to the surface lattice oxygen (O^{2-}, denoted as O_α) [41,42], the one at *ca.* 531.2 eV was assigned to adsorption oxygen at 531.0–531.2 eV (O- or/and O_2^{2-}, denoted as O_β) whereas the one at *ca.* 532.9 was assigned to hydroxyl at 532.7–532.9 eV (OH-, denoted as O_γ) [43–45], respectively. The details were depicted in Fig. 3. In addition, the Mn 2p spectra could be divided into two peaks which represented Mn^{3+} at 641.8–642.0 eV and Mn^{4+} at 643.6–643.9 eV [46,47].

The quantitative analysis was carried out and the results were reported in Table 3. Generally, the adsorbed oxygen species including O_β and O_γ was more active than O_α in oxidation reaction and a higher proportion of O_β and O_γ can promote the oxidation of NO to NO_2 at low temperature, which was beneficial to the occurrence of fast-SCR reaction at low temperature [46,48]. But it was reported that the activation capacity of NH_3 was positively correlated with the surface lattice oxygen activity [49–51]. Compared with the undoped MOs catalyst, the O_α concentration and binding energy for the Ni doped catalysts were significantly lower. The concentration of adsorbed oxygen in MOs was 0.64 while that of NMOs was 0.33−0.45. The Ni-doped catalysts showed considerably high proportion of Mn^{4+}, which was consistent with the literature on the Ni doping on the valence state of Mn in MnOx-based catalyst [52], indicating that there were certain interaction between Ni and Mn elements.

3.4. Acidity by NH_3-TPD

The adsorption and activation capacity of NH_3 were related to the surface acidity and redox ability [27]. NH_3-temperature programmed desorption (NH_3-TPD) was used to analyze the surface acidity, and results were shown in Fig. 4. The four catalysts had wide NH_3 desorption interval between 75−335 °C. The area of NH_3 desorption peak (see Table S2) showed a downward trend due to the addition of Ni, it significantly reduced especially for NMOs-4 and NMOs-6 catalysts, implying that the NH_3 adsorption capacity was lowered. Obviously, the Ni doping and content regulation can effectively tune the amount of acid sites. On the other hand, the incorporation of Ni had little effect on the surface acid strength when the Ni loading was low. The acid strength of NMOs-6 catalyst slightly increased due to the new acid sites which were brought by more Ni-containing species on catalyst surface [53].

3.5. Redox property

The redox ability of catalysts was characterized by H_2-temperature programmed reduction (H_2-TPR), the hydrogen consumption curves were recorded and shown in Fig. 5. Combining the results of XRD and FT-IR, the board reduction peak of MOs catalyst in 200−400 °C was mainly due to the reduction of $Mn^{4+}\rightarrow Mn^{3+}\rightarrow Mn^{2+}$ in cryptomelane-type manganese oxide (Part-1 and Part-2) [15,54–56]. The high temperature H_2 consumption peaks (Part-3) were only presented in Ni-doped catalysts, and the peak area increased with the increase of Ni loading (see Table 2 for more details). This peak may be attributed to the superposition of reduction peak of NiO and MnOx [57] or Ni-Mn composite oxides [58]. The starting temperature of the reduction process for the all catalysts were nearly identical (*ca.* 150 °C), suggesting the similar surface chemisorption oxygen activity. However, the reduction peak areas of the Ni-doped catalysts varied 23.0%–46.7% which was lower than that of MOs catalyst, especially the reducibility of surface lattice oxygen species decreased with the increase of Ni content. This indicated that the Ni-doping lowered the activity of the surface lattice oxygen and the redox ability [6]. The results were good agreement with the

Table 2
Bulk and surface element composition.

Catalysts	Bulk element concentration (EDS)				Surface element concentration (XPS)				
	K	Mn	Ni	Ni/Mn	K	Mn	Ni	O	Ni/Mn
MOs	3.9	30.7	0	0	3.0	27.8	0	68.4	0
NMOs-1	2.3	32.6	1.6	0.05	2.1	28.6	1.3	70.1	0.05
NMOs-4	0.5	26.4	4.0	0.16	0	25.0	4.7	72.3	0.19
NMOs-6	0.2	27.4	6.5	0.24	0	17.4	6.1	76.2	0.35

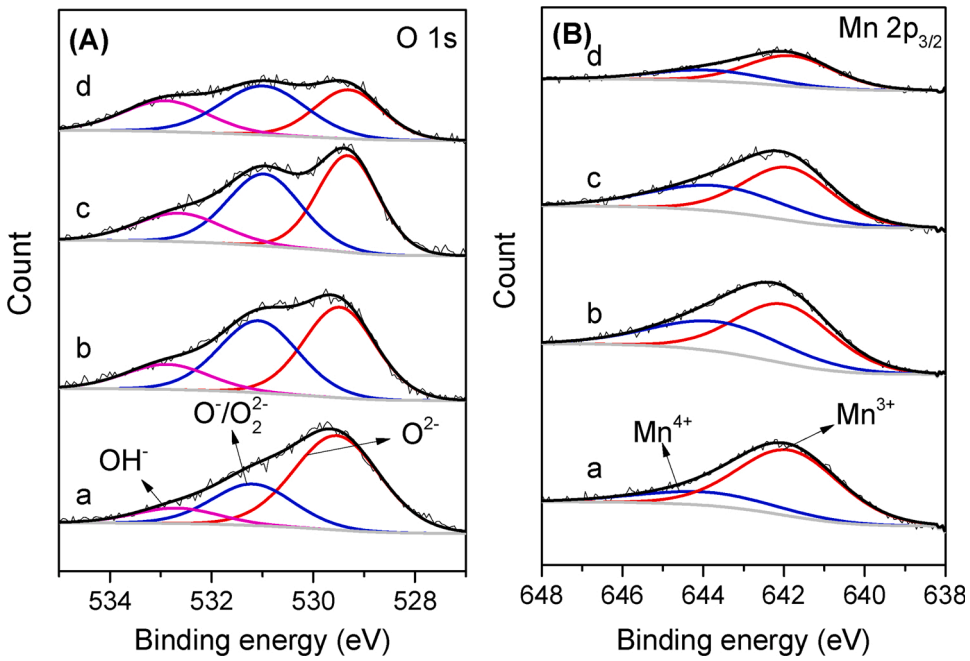

Fig. 3. XPS O 1s (A) and Mn 2p (B) spectra of catalysts (a: MOs, b: NMOs-1, c: NMOs-4 and d: NMOs-6).

Table 3
Mn and O binding energy of catalysts.

Catalysts	Binding energy, eV		$Mn^{4+}/(Mn^{3+}+Mn^{4+})$	Binding energy, eV			$(O_\beta+O_\gamma)/(O_\alpha+O_\beta+O_\gamma)$
	Mn^{3+}	Mn^{4+}		O_α	O_β	O_γ	
MOs	641.9	643.9	0.21	529.5	531.2	532.7	0.64
NMOs-1	642.0	643.6	0.41	529.5	531.1	532.9	0.45
NMOs-4	641.9	643.7	0.42	529.3	531.0	532.7	0.43
NMOs-6	641.8	643.9	0.31	529.3	531.0	532.9	0.33

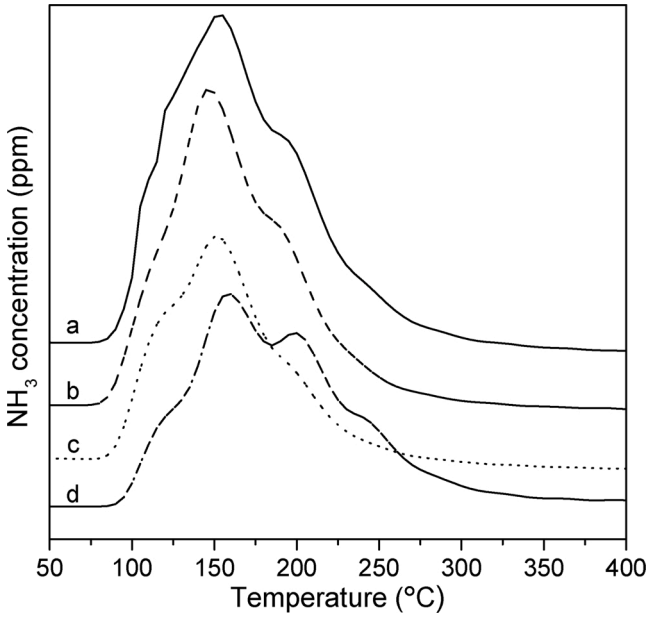

Fig. 4. NH_3-TPD profiles of catalysts (a: MOs, b: NMOs-1, c: NMOs-4 and d: NMOs-6).

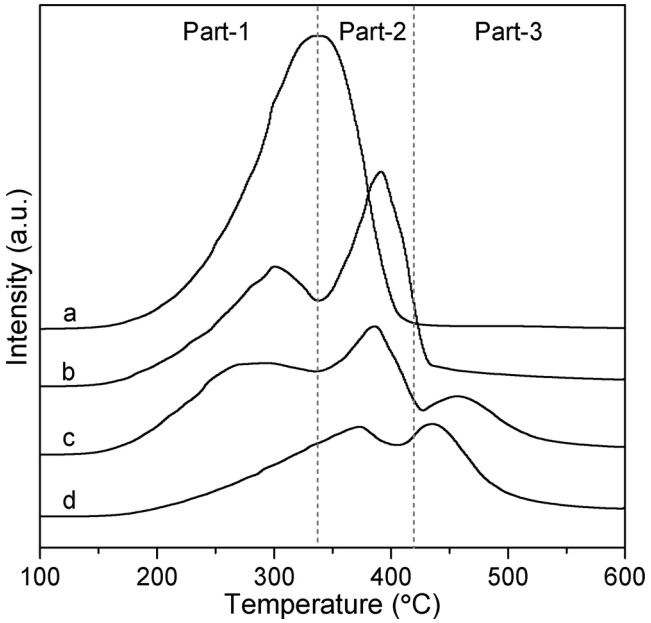

Fig. 5. H_2-TPR profiles of catalysts (a: MOs, b: NMOs-1, c: NMOs-4 and d: NMOs-6).

conclusion of XPS.

The direct oxidation of NH_3 was performed between 100 and 350 ℃ with a fixed WHSV of 30,000 mL/g h the results in Fig. S2 showed that NH_3 could be fully converted under the reaction conditions. In order to evaluate the low temperature activity of NH_3 oxidation of the four catalysts, the reaction was further carried out at 150 °C with a higher WHSV of 60,000 mL/g h The conversion of NH_3 over the different was depicted in Fig. 6. NH_3 was fully converted over MOs at this temperature, while 98.0 %, 92.8 % and 87.2 % of NH_3 conversion were obtained on NMOs-1, NMOs-4 and NMOs-6, respectively. The results showed that the incorporation of Ni weakened the lattice oxygen activity and reduced the amount of surface acid sites, which can effectively reduce the direct oxidation ability of the catalyst to NH_3.

3.6. NH_3-SCR activity and stability tests

The denitrification activity was carried out in the temperature range of 100–350 ℃ with a WHSV of 30,000 mL/g h and the results were depicted in Fig. 7A. MOs catalyst synthesized by solvent-free method exhibited excellent low temperature denitrification activity with a NO conversion of more than 99.6 % at 100–200 ℃, NO conversion gradually decreased till 26.1 % as the reaction temperature continued rising up to 350 °C. While the sample MO-HT prepared by hydrothermal method showed a sharp increase of NO conversion from *ca.* 15 % to *ca.* 95 % when temperature varied from 100 to 200 °C, then stabilized at this level till 300 °C, exhibiting better medium/high temperature performance. The calcined catalysts MOs-T (T = 300, 350, 400 and 500 ℃) revealed the similar catalytic activity results (not shown here) as MOs (Supporting information Fig. S3), indicating that the activity degradation of NH_3-SCR at medium/high temperature region (>200 ℃) was not due to the destruction of catalyst structure or surface physicochemical properties. When the WHSV increased by 3 times to 120,000 mL/g h the NO conversion at 100–200 ℃ on MOs could be still maintained at *ca.* 90 % although the high WHSV made it decay a little bit. On the other hand, MO-HT catalyst showed its low tolerance to the high WHSV, the NO conversion lost considerably during the tested temperature range, typically dropped from 90.7 % down to 43.5 % (Fig. 7B) at 200 °C. These results indicated that the MOs catalyst synthesized by solvent-free method had better low temperature denitrification performance in wide range of WHSV, which was probably caused the stable structure of cryptomelane-type manganese oxide. The medium/high temperature performance needed to be further improved.

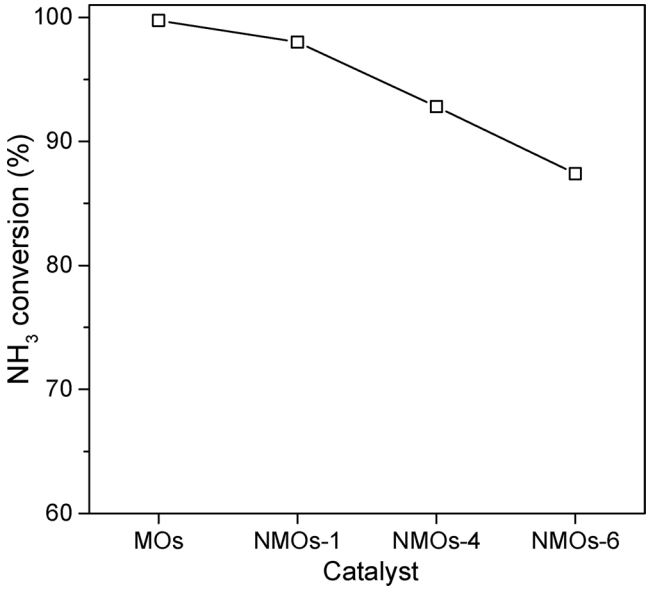

Fig. 6. NH_3 oxidation activity (in NH_3+O_2) on MOs and Ni-doped NMOs catalysts.
Reaction Conditions : Temperature = 150 ℃, [NH_3] = 500 ppm, [O_2] = 5 vol. %, WHSV = 60,000 mL/g h

The addition of appropriate promotor provides an efficient method to adjust the physical and chemical properties of the catalyst, such as redox and surface acidity [22,59,60]. In this work, a varied amount of Ni was introduced into the MnOx to improve the medium temperature (200–300 ℃) NH_3-SCR activity. It was found that the Ni loading was directly related to the NH_3-SCR activity of the catalyst at low and medium temperature (Supporting information Fig. S4). The influence of Ni loading on catalytic activity was depicted in Fig. 8. The NO conversion on MOs, NMOs-1 and NMOs-4 catalysts at low temperature (100–200 ℃) were all close to 100 %. The medium temperature (200–300 ℃) activity was improved due to the introduction of Ni species. The NO conversion over NMOs-1 increased by 17.1%–71.5% compared to that of MOs catalyst at the temperature of 300 ℃. It still had 87.2 % of NO conversion over the sample NMOs-4 at the same temperature, the maximum value among the all catalysts. Obviously, there was an optimal Ni loading for NMOs catalyst. Although the excessive Ni-doped NMOs-6 catalyst also showed an improvement at 300 ℃, its low temperature activity was rather poor, especially at 100 ℃ only 92.0 % of NO conversion was obtained. The N_2 selectivity over MOs and NMOs catalysts was shown in Fig. S5). Therefore, it can be found that solvent-free Ni-doping and optimizing the Ni loading were beneficial to broaden the NH_3-SCR active temperature region of MnOx-based catalysts. NH_3-SCR active temperature region of all catalysts showed in Table 1. The loading of Ni existed an optimal value as in NMOs-4 over which T_{95} increased by 40 ℃ from 100−225 ℃ to 100−265 ℃.

The long-term stability test was carried out on NMOs-4 catalyst at 240,000 mL/g h It was clear from Fig. 9 that the NO conversion maintained at 50–60 % during the tested range of 3000 min. The result suggested that the Ni-doping MnOx-based catalysts by solvent-free method could achieve good long-term stability in removing NOx.

4. Discussion

The NH_3 adsorption and activation capacity were related to the low temperature and medium/high temperature NH_3-SCR activity. Higher redox performance was conducive to the cleavage of N—H bonds, and surface acid site could be used for NH_3 adsorption [27]. Moderate NH_3 activation to form -NH_2 can further react with gas phase NO or adsorbed nitrate species to produce product N_2. Excessive NH_3 adsorption activation to form -NH or -N would cause NH_3 direct oxidation or non-selective oxidation reaction with NO species, resulting in a decrease in NO conversion and N_2 selectivity at medium/high temperature [61,62]. The addition of Ni promoted the transformation of pore structure from sheet-like to ink bottle-like, the uniformity was evidently modified. At the meantime, it was also important to note that the pore size was tuned by simply changing the loading of Ni according to N_2 adsorption/desorption analysis. However, Ni species were not detected by XRD for the all Ni contained samples, implying the amorphous state of those or the incorporation into cryptomelane-type manganese oxide crystallite through partial substitution of Mn. On the other hand, great changes took place on catalyst surface because of the introduction of Ni, it expelled surface K element to bulk, giving a Ni-rich K-leaned even K-free surface upon the Ni loading in catalyst. XRD and FT-IR results showed that the MOs catalyst synthesized by solvent-free method belonged to cryptomelane-type manganese oxide crystalline phase which was kept well even different quantity of Ni species were introduced. This resulting cryptomelane-type structure catalyst mostly determined the low temperature activity for NO removal. Moreover, Ni content was a simple factor to tune the redox ability and the surface acidity both of which were usually related to the medium/high temperature activity. When correlating these key factors and catalytic activity as a function of surface Ni/Mn ratio in Fig. 10, it could be clearly seen that the redox ability showed roughly a decreasing trend as Ni/Mn ratio increased from 0 for

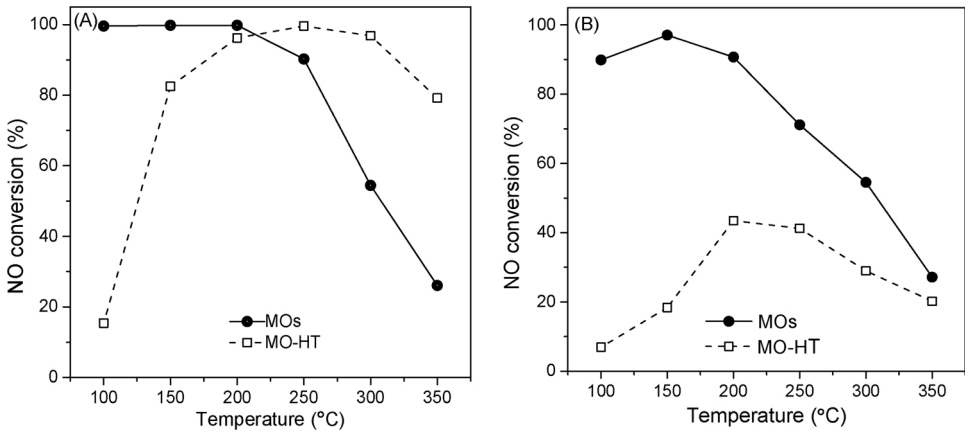

Fig. 7. The influence of WHSV on NH_3-SCR activity over MO-HT and MOs catalysts.
Reaction Conditions : [NO]=[NH_3] = 500 ppm, [O_2] = 5 vol.%, (A) WHSV = 30,000 mL/g h and (B) WHSV = 120,000 mL/g h

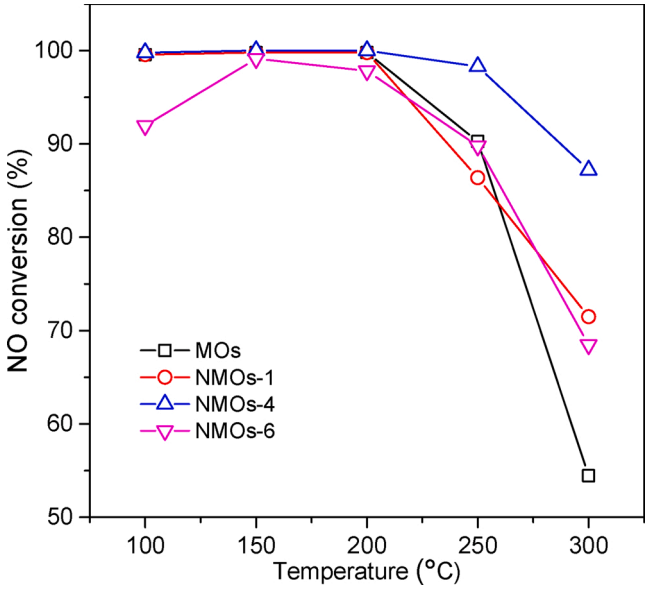

Fig. 8. NH_3-SCR activity of MOs and Ni-doped NMOs catalysts.
Reaction Conditions : [NO]=[NH_3] = 500 ppm, [O_2] = 5 vol.%, WHSV = 30,000 mL/g h

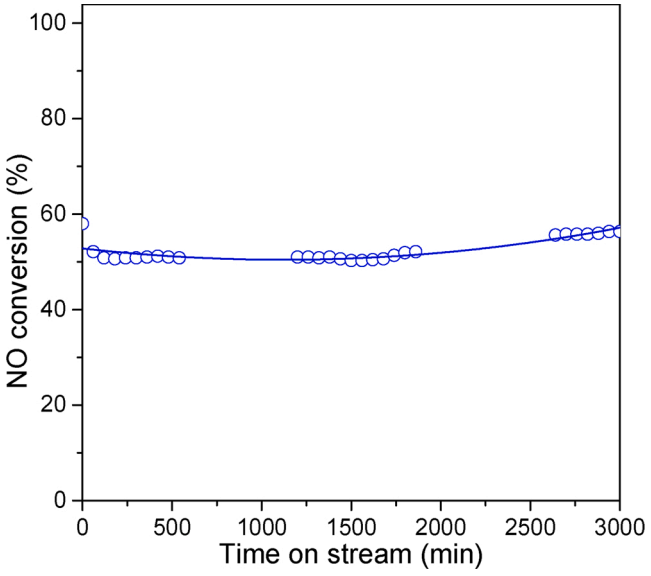

Fig. 9. Catalytic stability test over NMOs-4 catalyst.
Reaction Conditions : [NO]=[NH_3] = 500 ppm, [O_2] = 5%, WHSV=240,000 mL/g h Temperature = 200 ℃

MOs to 0.39 for NMOs-6, correspondingly, the NH_3 direct oxidation activity lost gradually.

The Ni-doping reduced the content of K and Mn of catalysts according to the results of EDS and XPS. K species in the flue gas was often regarded as a catalyst poison because of the strongly competitive adsorption between it and NH_3. However, it acted as a promotor when K co-existed with α-MOx such as cryptomelane-type manganese oxides [63,64]. The electron donating effect of alkali metal K element was beneficial to activate the Mn-O bond [15,65,66], improving the redox property, which was beneficial to the activation of NH_3 [67,68]. The decreased binding energy of lattice oxygen gave the direct evidence, whereas the decrease of reducibility due to the decreased K content through the incorporation of Ni catalysts gave the indirect evidence according to XPS and H_2-TPR measurements. On the other hand, Ni species might also occupy defect sites in MnOx or partially replace Mn element, which enhanced the interaction between Ni and Mn in the catalyst, resulting a decrease in the mobility and activity of lattice oxygen. The H_2 consumption peak position moved to higher temperature side but the consumption became less, proving that the incorporation of Ni weakened the lattice oxygen activity of the catalyst, the direct

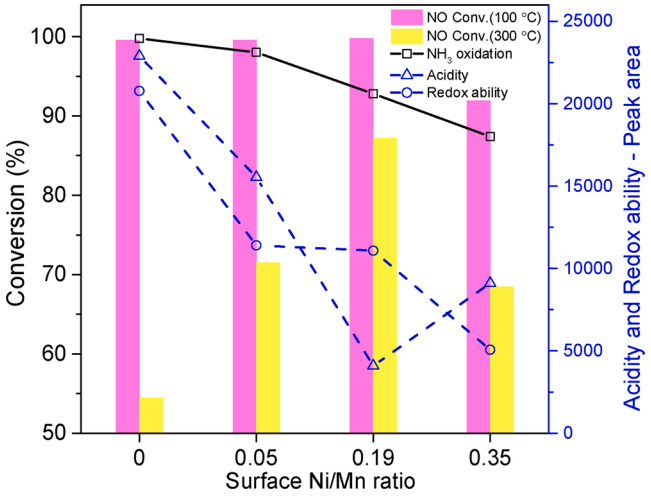

Fig. 10. The influence of Ni loading on redox ability and NH_3-SCR activity.

oxidation reaction of NH_3 at medium and high temperature was suppressed as a consequence [21].

Being different from the redox ability, the surface acidity dropped down firstly, got to the valley on NMOs-4, and then rose up. It was interesting to note from Fig. 10 that the medium temperature activity (orange bars) seemed to show the exact opposite trend among the Ni-doped catalyst, obtaining the best medium activity on NMOs-4. Appropriate amount of acidic sites was good to activate N-H of NH_3 at a certain extent rather than excessive activation which would drive the formation of -NH or -N, finally resulting in the NH_3 oxidation or non-selective oxidation reaction with NO. In fact, although NMOs-6 possessed more surface acid sites than NMOs-4, the NH_3 oxidation activity was worse, which was likely related to the low surface content of Mn species [53]. One can state from these results that both redox and acidity were important factors that can influence the catalytic performance of NOx removal, only well-coordinated redox and acidity can improve the medium/high temperature performance. Therefore, it could be considered that the regulation of the Ni loading adjusted the surface acidity and redox properties of the catalysts, so that the catalysts had moderate NH_3 adsorption and activation capacity, and realized the high NH_3-SCR activity at low and medium temperature.

5. Conclusion

NMOs NH_3-SCR catalysts were synthesized by solvent-free transition metal doping method to get the cryptomelane-type crystalline structure which was mainly responsible for low temperature activity. The introduction of Ni can effectively improve the denitrification performance at medium/high temperature thanks to modified redox and acidity properties by simply changing the Ni content. Ni species partially substituted K and Mn, thus weakening the surface lattice oxygen activity and reducing the number of surface acid sites, which could be proved by oxidation of NH_3 at high temperature. Appropriate NH_3 adsorption and activation capacity were the key to enlarge the NH_3-SCR active temperature region. Its essence was to break the balance between SCR reaction and NH_3 direct oxidation reaction at medium and high SCR reaction temperature. The NO conversion at 100–250 ℃ was more than 98.3 %, it increased by 32.8 % from 54.4% to 87.2% at medium temperature over NMOs-4 (T_{95} = 100−265 ℃).

Funding

This work was financially supported by the National Natural Science Foundation of China (No. 21872098).

CRediT authorship contribution statement

Hui Kang: Conceptualization, Writing - original draft. **Jiajie Wang:** Resources. **Jian Zheng:** Writing - reviewg & editing. **Wei Chu:** Investigation, Methodology. **Changjin Tang:** Validation, Data curation. **Ji Jiawei:** Resources. **Rui Ren:** Validation, Data curation. **Mengxia Wu:** Formal analysis. **Fangli Jing:** Conceptualization, Supervision.

Declaration of Competing Interest

The authors declare that they have no known competing financial interests or personal relationships that could have appeared to influence the work reported in this paper.

Appendix A. Supplementary data

Supplementary material related to this article can be found, in the online version, at doi:https://doi.org/10.1016/j.mcat.2020.111376.

References

[1] A. Richter, J.P. Burrows, H. Nuss, C. Granier, U. Niemeier, Increase in tropospheric nitrogen dioxide over China observed from space, Nature 437 (2005) 129–132.
[2] T.-M. Fu, Y. Zheng, F. Paulot, J. Mao, R.M. Yantosca, Positive but variable sensitivity of August surface ozone to large-scale warming in the southeast United States, Nature Clim. Change 5 (2015) 454–458.
[3] N.Y. Topsoe, Mechanism of the selective catalytic reduction of nitric-oxide by ammonia elucidated by in-situ online fourier-transform infrared-spectroscopy, Science 265 (1994) 1217–1219.
[4] V.I. Parvulescu, P. Grange, B. Delmon, Catalytic removal of NO, Catal. Today 46 (1998) 233–316.
[5] L. Han, S. Cai, M. Gao, J.-y. Hasegawa, P. Wang, J. Zhang, L. Shi, D. Zhang, Selective catalytic reduction of NOx with NH_3 by using novel catalysts: state of the art and future prospects, Chem. Rev. 119 (2019) 10916–10976.
[6] B. Shen, Y. Wang, F. Wang, T. Liu, The effect of Ce-Zr on NH_3-SCR activity over $MnOx(0.6)/Ce_{0.5}Zr_{0.5}O_2$ at low temperature, Chem. Eng. J. 236 (2014) 171–180.
[7] Z. Liu, Y. Yi, J. Li, S.I. Woo, B. Wang, X. Cao, Z. Li, A superior catalyst with dual redox cycles for the selective reduction of NOx by ammonia, Chem. Commun. 49 (2013) 7726–7728.
[8] H. Xu, J. Liu, Z. Zhang, S. Liu, Q. Lin, Y. Wang, S. Dai, Y. Chen, Design and synthesis of highly-dispersed WO_3 catalyst with highly effective NH_3-SCR activity for NO_X abatement, ACS Catal. 9 (2019) 11557–11562.
[9] F. Liu, H. He, C. Zhang, Z. Feng, L. Zheng, Y. Xie, T. Hu, Selective catalytic reduction of NO with NH_3 over iron titanate catalyst: catalytic performance and characterization, Appl. Catal. B Environ. 96 (2010) 408–420.
[10] X. Li, K. Li, Y. Peng, X. Li, Y. Zhang, D. Wang, J. Chen, J. Li, Interaction of phosphorus with a FeTiOx catalyst for selective catalytic reduction of NOx with NH_3: influence on surface acidity and SCR mechanism, Chem. Eng. J. 347 (2018) 173–183.
[11] V. Thanh Huyen, J. Radnik, E. Kondratenko, M. Schneider, U. Armbruster, A. Brueckner, Structure-reactivity relationships in $VO_x/Ce_xZr_{1-x}O_2$ catalysts used for low-temperature NH_3-SCR of NO, Appl. Catal. B-Environ. 197 (2016) 159–167.
[12] Z. Wu, B. Jiang, Y. Liu, H. Wang, R. Jin, DRIFT study of manganese/titania-based catalysts for low-temperature selective catalytic reduction of NO with NH_3, Environ. Sci. Technol. 41 (2007) 5812–5817.
[13] W.S. Kijlstra, D.S. Brands, E.K. Poels, A. Bliek, Mechanism of the selective catalytic reduction of NO by NH_3 over $MnOx/Al_2O_3$ .1. Adsorption and desorption of the single reaction components, J. Catal. 171 (1997) 208–218.
[14] D.A. Pena, B.S. Uphade, E.P. Reddy, P.G. Smirniotis, Identification of surface species on titania-supported manganese, chromium, and copper oxide low-temperature SCR catalysts, J. Phys. Chem. B 108 (2004) 9927–9936.
[15] C. Wang, L. Sun, Q. Cao, B. Hu, Z. Huang, X. Tang, Surface structure sensitivity of manganese oxides for low-temperature selective catalytic reduction of NO with NH_3, Appl. Catal. B 101 (2011) 598–605.
[16] M. Stanciulescu, G. Caravaggio, A. Dobri, J. Moir, R. Burich, J.P. Charland, P. Bulsink, Low-temperature selective catalytic reduction of NOx with NH_3 over Mn-containing catalysts, Appl. Catal. B-Environ. 123 (2012) 229–240.
[17] Y. Xin, H. Li, N. Zhang, Q. Li, Z. Zhang, X. Cao, P. Hu, L. Zheng, J.A. Anderson, Molecular-level insight into selective catalytic reduction of NOx with NH_3 to N_2 over a highly efficient bifunctional V-alpha-MnOx catalyst at low temperature, ACS Catal. 8 (2018) 4937–4949.
[18] J. Liu, Y. Wei, P.-Z. Li, P. Zhang, W. Su, Y. Sun, R. Zou, Y. Zhao, Experimental and theoretical investigation of mesoporous MnO_2 nanosheets with oxygen vacancies for high-efficiency catalytic DeNO(x), ACS Catal. 8 (2018) 3865–3874.
[19] Z. Huang, X. Gu, W. Wen, P. Hu, M. Makkee, H. Lin, F. Kapteijn, X. Tang, A "smart" hollandite deNOx catalyst: self-protection against alkali poisoning, Angew. Chem. Int. Ed. 52 (2013) 660–664.
[20] T.S. Park, S.K. Jeong, S.H. Hong, S.C. Hong, Selective catalytic reduction of nitrogen oxides with NH_3 over natural manganese ore at low temperature, Ind. Eng. Chem. Res. 40 (2001) 4491–4495.
[21] S. Deng, T. Meng, B. Xu, F. Gao, Y. Ding, L. Yu, Y. Fan, Advanced $MnOx/TiO_2$ catalyst with preferentially exposed anatase {001} facet for low-temperature SCR of NO, ACS Catal. 6 (2016) 5807–5815.
[22] X. Wang, X. Li, Q. Zhao, W. Sun, M. Tade, S. Liu, Improved activity of W-modified MnO_x-TiO_2 catalysts for the selective catalytic reduction of NO with NH_3, Chem. Eng. J. 288 (2016) 216–222.
[23] Y. Shen, Y. Su, Y. Ma, Transition metal ions regulate the catalytic performance of $Ti_{0.8}M_{0.2}Ce_{0.2}O_{2+x}$ for the NH_3-SCR of NO: The acidic mechanism, RSC Adv. 5 (2015) 7597–7603.
[24] S. Yang, C. Liu, H. Chang, L. Ma, Z. Qu, N. Yan, C. Wang, J. Li, Improvement of the activity of gamma-Fe_2O_3 for the selective catalytic reduction of NO with NH_3 at high temperatures: NO reduction versus NH_3 oxidization, Ind. Eng. Chem. Res. 52 (2013) 5601–5610.
[25] F. Liu, K. Asakura, H. He, W. Shan, X. Shi, C. Zhang, Influence of sulfation on iron titanate catalyst for the selective catalytic reduction of NOx with NH_3, Appl. Catal. B 103 (2011) 369–377.
[26] L. Chen, X. Niu, Z. Li, Y. Dong, Z. Zhang, F. Yuan, Y. Zhu, Promoting catalytic performances of Ni-Mn spinel for NH_3-SCR by treatment with SO_2 and H_2O, Catal. Commun. 85 (2016) 48–51.
[27] W. Qu, X. Liu, J. Chen, Y. Dong, X. Tang, Y. Chen, Single-atom catalysts reveal the dinuclear characteristic of active sites in NO selective reduction with NH_3, Nat. Commun. 11 (2020).
[28] M. Zhu, J.-K. Lai, U. Tumuluri, Z. Wu, I.E. Wachs, Nature of active sites and surface intermediates during SCR of NO with NH_3 by supported V_2O_5–WO_3/TiO_2 catalysts, J. Am. Chem. Soc. 139 (2017) 15624–15627.

[29] Y.S. Ding, X.F. Shen, S. Sithambaram, S. Gomez, R. Kumar, V.M.B. Crisostomo, S. L. Suib, M. Aindow, Synthesis and catalytic activity of cryptomelane-type manganese dioxide nanomaterials produced by a novel solvent-free method, Chem. Mat. 17 (2005) 5382–5389.

[30] C. Almquist, M. Krekeler, L. Jiang, An investigation on the structure and catalytic activity of cryptomelane-type manganese oxide materials prepared by different synthesis routes, Chem. Eng. J. 252 (2014) 249–262.

[31] X. Hu, S. Li, Y. Chen, W. Qu, J. Chen, Z. Ma, X. Tang, Single-ion copper doping greatly enhances catalytic activity of manganese oxides via electronic interactions, Chem. Commun. (Camb.) 56 (2020) 904–907.

[32] Y. Yuan, S.M. Wood, K. He, W. Yao, D. Tompseett, J. Lu, A. Nie, M.S. Islam, R. Shahbazian-Yassar, Atomistic insights into the oriented attachment of tunnel-based oxide nanostructures, ACS Nano 10 (2016) 539–548.

[33] Q. Wu, X. Meng, X. Gao, F.-S. Xiao, Solvent-free synthesis of zeolites: mechanism and utility, Acc. Chem. Res. 51 (2018) 1396–1403.

[34] T. Gao, M. Glerup, F. Krumeich, R. Nesper, H. Fjellvag, P. Norby, Microstructures and spectroscopic properties of cryptomelane-type manganese dioxide nanofibers, J. Phys. Chem. C 112 (2008) 13134–13140.

[35] W.Y. Hernandez, M.A. Centeno, F. Romero-Sarria, S. Ivanova, M. Montes, J. A. Odriozola, Modified cryptomelane-type manganese dioxide nanomaterials for preferential oxidation of CO in the presence of hydrogen, Catal. Today 157 (2010) 160–165.

[36] Z. Yan, S. Liu, Y. Zhang, T. Wang, S. Luo, W. Chu, F. Jing, The role of Zr in NiZrAl oxides catalyst and the evaluation on steam reforming of glycerol for hydrogen product, Catal. Today 319 (2019) 229–238.

[37] K. Ralphs, C. Hardacre, S.L. James, Application of heterogeneous catalysts prepared by mechanochemical synthesis, Chem. Soc. Rev. 42 (2013) 7701–7718.

[38] Y. Yang, S. Zhang, S. Wang, K. Zhang, H. Wang, J. Huang, S. Deng, B. Wang, Y. Wang, G. Yu, Ball milling synthesized MnOx as highly active catalyst for gaseous POPs removal: significance of mechanochemically induced oxygen vacancies, Environ. Sci. Technol. 49 (2015) 4473–4480.

[39] T. Gu, Y. Liu, X. Weng, H. Wang, Z. Wu, The enhanced performance of ceria with surface sulfation for selective catalytic reduction of NO by NH_3, Catal. Commun. 12 (2010) 310–313.

[40] Z. Ye, T. Li, G. Ma, Y. Dong, X. Zhou, Metal-Ion (Fe, V, Co, and Ni)-Doped MnO_2 Ultrathin Nanosheets Supported on Carbon Fiber Paper for the Oxygen Evolution Reaction, Adv. Funct. Mater. 27 (2017).

[41] K. Zha, C. Feng, L. Han, H. Li, T. Yan, S. Kuboon, L. Shi, D. Zhang, Promotional effects of Fe on manganese oxide octahedral molecular sieves for alkali-resistant catalytic reduction of NOx: XAFS and in situ DRIFTs study, Chem. Eng. J. 381 (2020).

[42] S. Liu, Z. Yan, Y. Zhang, R. Wang, S.-Z. Luo, F. Jing, W. Chu, Carbon nanotubes supported nickel as the highly efficient catalyst for hydrogen production through glycerol steam reforming, ACS Sustain. Chem. Eng. 6 (2018) 14403–14413.

[43] M.C. Biesinger, B.P. Payne, A.P. Grosvenor, L.W.M. Lau, A.R. Gerson, R.S.C. Smart, Resolving surface chemical states in XPS analysis of first row transition metals, oxides and hydroxides: Cr, Mn, Fe, Co and Ni, Appl. Surf. Sci. 257 (2011) 2717–2730.

[44] F. Gao, X. Tang, H. Yi, J. Li, S. Zhao, J. Wang, C. Chu, C. Li, Promotional mechanisms of activity and SO_2 tolerance of Co- or Ni-doped MnOx-CeO_2 catalysts for SCR of NOx with NH_3 at low temperature, Chem. Eng. J. 317 (2017) 20–31.

[45] J.C. Dupin, D. Gonbeau, P. Vinatier, A. Levasseur, Systematic XPS studies of metal oxides, hydroxides and peroxides, PCCP 2 (2000) 1319–1324.

[46] S. Cai, D. Zhang, L. Shi, J. Xu, L. Zhang, L. Huang, H. Li, J. Zhang, Porous Ni-Mn oxide nanosheets in situ formed on nickel foam as 3D hierarchical monolith de-NOx catalysts, Nanoscale 6 (2014) 7346–7353.

[47] D. Meng, W. Zhan, Y. Guo, Y. Guo, L. Wang, G. Lu, A highly effective catalyst of Sm-MnOx for the NH_3-SCR of NOx at low Temperature: promotional role of Sm and its catalytic performance, ACS Catal. 5 (2015) 5973–5983.

[48] Y. Liu, J. Xu, H. Li, S. Cai, H. Hu, C. Fang, L. Shi, D. Zhang, Rational design and in situ fabrication of MnO_2@$NiCo_2O_4$ nanowire arrays on Ni foam as high-performance monolith de-NOx catalysts, J. Mater. Chem. A 3 (2015) 11543–11553.

[49] W. Zhu, X. Tang, F. Gao, H. Yi, R. Zhang, J. Wang, C. Yang, S. Ni, The effect of non-selective oxidation on the $Mn_2Co_1O_x$ catalysts for NH_3-SCR: positive and non-positive, Chem. Eng. J. 385 (2020).

[50] P. Hu, M.E. Schuster, Z. Huang, F. Xu, S. Jin, Y. Chen, W. Hua, D.S. Su, X. Tang, The active sites of a rod-shaped hollandite deNO(x) catalyst, Chem. Eur. J. 21 (2015) 9619–9623.

[51] K. Cheng, B. Liu, W. Song, J. Liu, Y. Chen, Z. Zhao, Y. Wei, Effect of Nb promoter on the structure and performance of iron titanate catalysts for the selective catalytic reduction of NO with NH_3, Ind. Eng. Chem. Res. 57 (2018) 7802–7810.

[52] B. Thirupathi, P.G. Smirniotis, Nickel-doped Mn/TiO_2 as an efficient catalyst for the low-temperature SCR of NO with NH_3: catalytic evaluation and characterizations, J. Catal. 288 (2012) 74–83.

[53] P.G. Smirniotis, D.A. Pena, B.S. Uphade, Low-temperature selective catalytic reduction (SCR) of NO with NH_3 by using Mn, Cr, and Cu oxides supported on Hombikat TiO_2, Angew. Chem. Int. Ed. 40 (2001) 2479-+.

[54] G. Yang, H. Zhao, X. Luo, K. Shi, H. Zhao, W. Wang, Q. Chen, H. Fan, T. Wu, Promotion effect and mechanism of the addition of Mo on the enhanced low temperature SCR of NOx by NH_3 over MnOx/gamma-Al_2O_3 catalysts, Appl. Catal. B 245 (2019) 743–752.

[55] L. Qu, C. Li, G. Zeng, M. Zhang, M. Fu, J. Ma, F. Zhan, D. Luo, Support modification for improving the performance of MnOx-CeOy/gamma-Al_2O_3 in selective catalytic reduction of NO by NH_3, Chem. Eng. J. 242 (2014) 76–85.

[56] X. Liu, S. Jiang, H. Li, J. Yang, Z. Yang, J. Zhao, H. Peng, K. Shih, Elemental mercury oxidation over manganese oxide octahedral molecular sieve catalyst at low flue gas temperature, Chem. Eng. J. 356 (2019) 142–150.

[57] Y. Han, J. Mu, X. Li, J. Gao, S. Fan, F. Tan, Q. Zhao, Triple-shelled $NiMn_2O_4$ hollow spheres as an efficient catalyst for low-temperature selective catalytic reduction of NOx with NH_3, Chem. Commun. 54 (2018) 9797–9800.

[58] Y. Wan, W. Zhao, Y. Tang, L. Li, H. Wang, Y. Cui, J. Gu, Y. Li, J. Shi, Ni-Mn bi-metal oxide catalysts for the low temperature SCR removal of NO with NH_3, Appl. Catal. B-Environ. 148 (2014) 114–122.

[59] F. Gao, X. Tang, H. Yi, J. Li, S. Zhao, J. Wang, C. Chu, C. Li, Promotional mechanisms of activity and SO_2 tolerance of Co-or Ni-doped MnOx-CeO_2 catalysts for SCR of NOx with NH_3 at low temperature, Chem. Eng. J. 317 (2017) 20–31.

[60] H. Li, D. Zhang, P. Maitarad, L. Shi, R. Gao, J. Zhang, W. Cao, In situ synthesis of 3D flower-like NiMnFe mixed oxides as monolith catalysts for selective catalytic reduction of NO with NH_3, Chem. Commun. 48 (2012) 10645–10647.

[61] H. Yuan, N. Sun, J. Chen, J. Jin, H. Wang, P. Hu, Insight into the NH_3-assisted selective catalytic reduction of NO on beta-MnO_2(110): reaction mechanism, activity descriptor, and evolution from a pristine state to a steady state, ACS Catal. 8 (2018) 9269–9279.

[62] A. Marberger, D. Ferri, M. Elsener, O. Krocher, The significance of lewis acid sites for the selective catalytic reduction of nitric oxide on vanadium-based catalysts, Angew. Chem. Int. Ed. 55 (2016) 11989–11994.

[63] Z. Huang, H. Li, J. Gao, X. Gu, L. Zheng, P. Hu, Y. Xin, J. Chen, Y. Chen, Z. Zhang, J. Chen, X. Tang, Alkali- and sulfur-resistant tungsten-based catalysts for NOx emissions control, Environ. Sci. Technol. 49 (2015) 14460–14465.

[64] M. Kong, Q. Liu, J. Zhou, L. Jiang, Y. Tian, J. Yang, S. Ren, J. Li, Effect of different potassium species on the deactivation of V_2O_5-WO_3/TiO_2 SCR catalyst: comparison of K_2SO_4, KCl and K_2O, Chem. Eng. J. 348 (2018) 637–643.

[65] J. Hou, L. Liu, Y. Li, M. Mao, H. Lv, X. Zhao, Tuning the K^+ concentration in the tunnel of OMS-2 nanorods leads to a significant enhancement of the catalytic activity for benzene oxidation, Environ. Sci. Technol. 47 (2013) 13730–13736.

[66] Z. Hao, Z. Shen, Y. Li, H. Wang, L. Zheng, R. Wang, G. Liu, S. Zhan, The role of alkali metal α-MnO_2 catalyzed ammonia-selective catalysis, Angew. Chem. Int. Ed. 58 (2019) 6351–6356.

[67] T. Hamaguchi, T. Tanaka, N. Takahashi, Y. Tsukamoto, N. Takagi, H. Shinjoh, Low-temperature NO-adsorption properties of manganese oxide octahedral molecular sieves with different potassium content, Appl. Catal. B-Environ. 193 (2016) 234–239.

[68] F. Xu, Z. Huang, P. Hu, Y. Chen, L. Zheng, J. Gao, X. Tang, The promotion effect of isolated potassium atoms with hybridized orbitals in catalytic oxidation, Chem. Commun. 51 (2015) 9888–9891.